THE EFFECT OF SELECTIVE LASER MELTING TECHNOLOGY ON THE DEVELOPMENT OF THE STRUCTURE OF SAMPLES MADE FROM WC-CO POWDER

David Bricin*, Andrea Elmanova, Antonin Kriz

Department of Material Science and Technology, University of West Bohemia in Pilsen, Univerzitni 8 301 00, Pilsen, Czech Republic

Abstract

The aim of this study was to analyse how changing the processing parameters of WC-Co powder affects its properties. The powder mixture properties were evaluated by technological tests firstly and then the results were than compared with properties of SD251 stainless steel powder which is commonly processed by the technology of selective laser melting (SLM). Different laser powers and laser spot feed rates were used for different samples. As a result, different values for the applied energy density Ev were obtained. The changes in the density, porosity and changes in the chemical and structural compositions of the printed samples were then evaluated using light and electron microscopy. This evaluation was supplemented by X-ray diffraction analysis of the phase composition and evaluation of mechanical properties using hardness testing. These experiments allowed us, for example, to determine the dependence of the density of the samples on the applied energy Ev. The maximum density of the printed samples was about 70%. In addition, metallographic analysis and X-ray diffraction analysis revealed the development of the eta phase in the specimens, and how changing the parameters changes the type and number of pores in the volume of the printed samples.

Keywords: *WC-Co Powder, SLM Technology, Porosity, phase evolution*

1. INTRODUCTION

WC-Co powder compounds are materials used mainly for the production of machine tools. Other important applications are for wear parts such as wire dies or nozzles. All these machine parts are characterized by their simple shape. This is because in most cases these machine parts are manufactured by compression and subsequent sintering techniques. *(Kríž and Bricín, 2017; Sarin, 2014)* When using conventional WC-Co powder processing techniques, it is known how their structure evolves based on their processing parameters. As a result, it is possible to change their mechanical and physical properties depending on how the processing parameters are changed. Nowadays, a wide variety of additive processing techniques are used. These techniques make use of the fact that it is very easy to create a machine part model using design software. The part is then divided into layers and these layers are then processed by various techniques and interconnected into a functional component. In this way, it is possible to create structurally unique machine parts with a complicated internal structure, which makes it possible for example to intensify its cooling or to reduce its weight without reducing its bearing capacity and shortening its service life. SLM technology is used to process steel powders and powders from non-ferrous metals. *(Venuvinod and Ma, 2010; Pacurar and Pacurar, 2016*) It has not been designed for processing WC-Co powders, but its use for WC-Co powder mixtures would allow the expansion of the range of manufactured products and modification of the existing ones, to extend their service life and control the conditions of their application. This could all be done using internal structures which can be created using SLM. For these reasons, this study has verified the workability of the selected WC-Co powder blend by SLM. The technological properties of the powder mixture were analysed and metallographic analysis was used to assess the suitability of this mixture for the SLM process. It was possible to assess its suitability for this process on prototype samples by comparing the initial state with the structural state created by SLM.

2. MATERIALS AND METHODS

2.1. Experimental material

WC-Co powder SD251 was chosen as the experimental material. This material was supplied by Global Tungsten Powders s.r.o. It consists of 12% Co binder, and the rest of the material is made up of tungsten carbide, which was verified by EDX analysis. This analysis was performed on the surface and a transverse metallographic cut across the powder particles, see Fig 1.

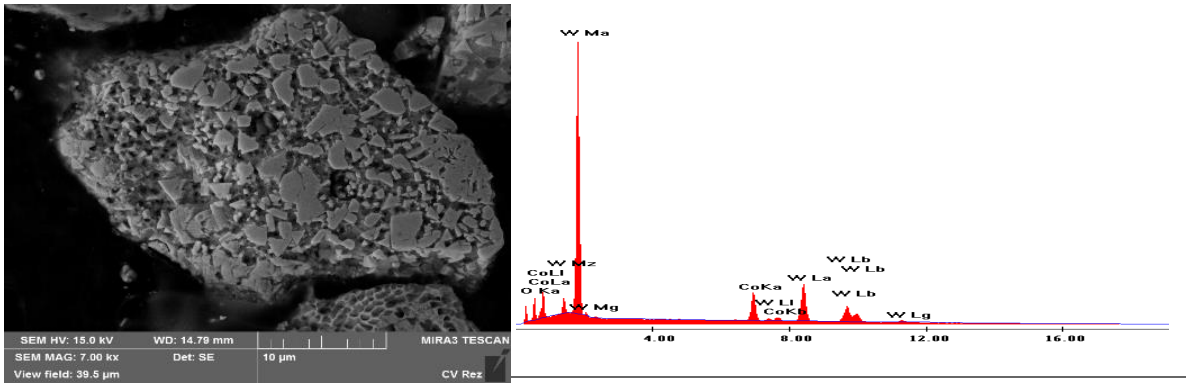

Element	W(C)	Co
Wt. %	87.57±0.61	12.43±0.61

Fig. 1. On the left is a cross-section of a powder particle. On the right is the chemical composition spectrum recorded for this material. The table shows the average values of the chemical composition of each of the powder particles.

In order to differentiate the structural phases from which the powder particles were composed, their phase composition was analysed. The phase composition of the powder particles was measured by X-ray diffraction analysis using the Bragg-Brentano method. For the subsequent evaluation of the distribution of the structural phases in the powder particles, they were etched to identify structural phases according to norm ASTM B657. *(18, 2019)* The results of these analyses are summarized below, see figures 2 and 3.

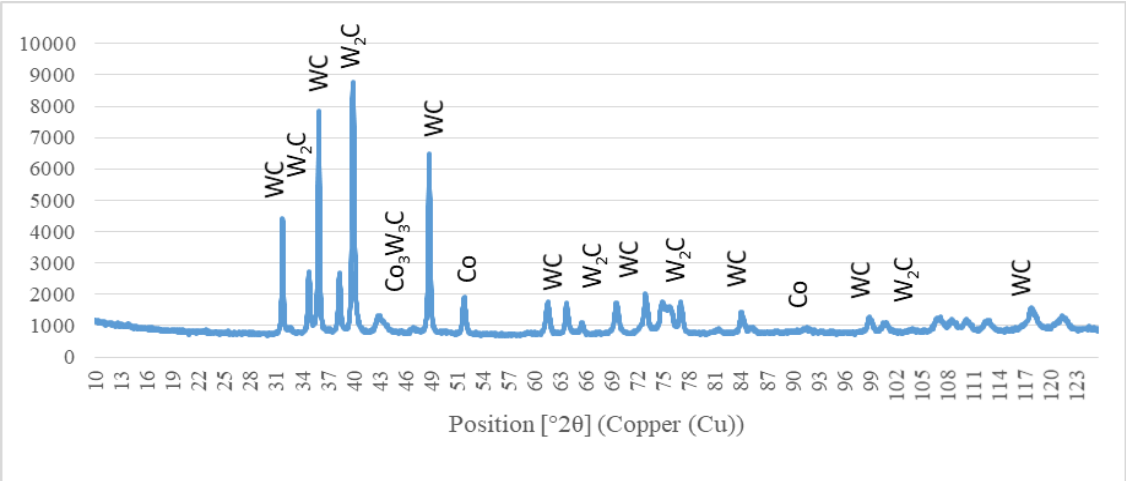

Fig. 2. Diffraction recording of the phase composition analysis performed on the particles of the powder mixture

From Fig. 2, it can be seen that the powder particles are composed of Co binder, grains of WC and W2C phase, and a Co3W3C phase. This structural composition was confirmed by metallographic analysis, see Fig. 3.

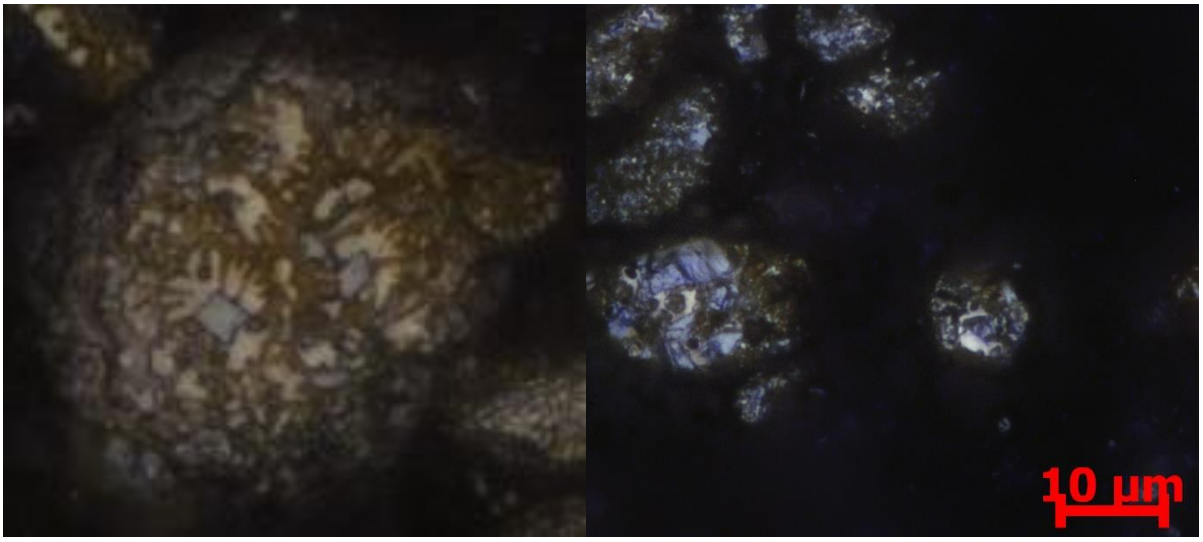

Fig. 3. Metallographic images of powder particle structure. The left part of the image shows the results of etching to identify the Co3W3C phase. The right part of the image shows the results of etching using Murakami reagent to identify the tungsten carbide and binder. The tungsten carbide phase is from light grey to blue. The binder is white. The Co3W3C phase is brown-orange. *(Bricin and Kriz, 2018)*

The presence of the Co3W3C phase in the powder particle structure is related to the method of making the powder mixture. It is possible to reduce the amount of this phase in the volume of the powder particles by changing the method of making of the powder.

From the WC-Co phase diagram (Fig 4), it can be seen that this structural phase arises when the stoichiometric content of carbon is lower than the amount of carbon dissolved in the intermediate phase of WC.

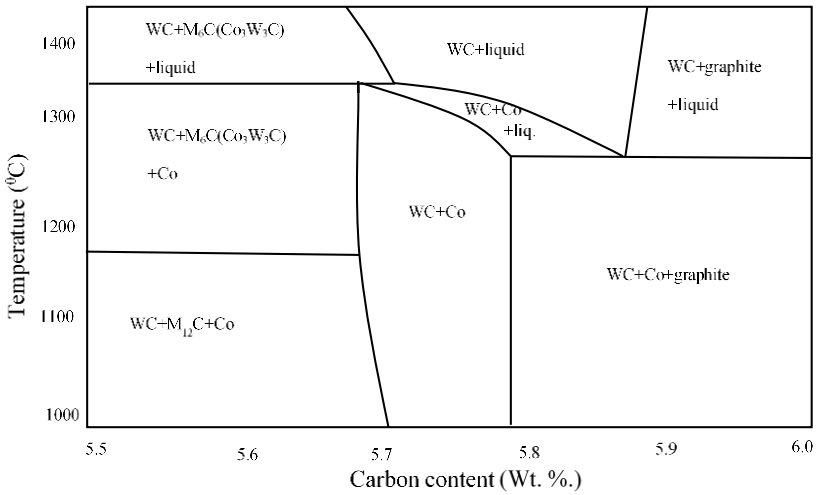

Fig. 4. WC-Co Binary diagram (*Sarin, 2014)*

Thus, the formation of this phase is related to the distribution and volume amount of carbon in the powder particles. If the amount of carbon is high enough, this phase evolution can be prevented by slow cooling of the material from the sintering temperature. In the case of the particles of the material to be analysed, the cooling rate was probably too high. Therefore, this phase initiated preferentially in areas where heat dissipation was most intense. These areas were the surfaces of the powder particles, see Figure 3.

The suitability of the powder blend for SLM was verified by the powder flowability test and powder spill test. *(Sutton et al., 2016)* The measured values were then compared to the values found for PH1 powder. This material was chosen for comparison because it is commonly used in SLM, and its properties are designed for use with this technology. The results of these tests are shown in Table 1 below.

Type of powder	**SD251**	**PH1**
Powder flowability (s/200g)	2.7±0.15	3.7±0.11
Bulk density (g/cm^3)	7.3±1.1	4.2±0.63
Average powder spread (Spill test) (mm)	1.9±0.41	3.5±0.54

Table 1. Results of analyses of technological properties of powder mixture SD251 and comparative material PH1

It can be seen from Table 1 that the WC-Co powder mixture has a poorer flowability of about 27% less than PH1 powder. In addition, the spillage test showed that the width of the trace formed is about 45% smaller for the SD251 powder blend than was measured for the PH1 powder. The advantage of the SD 251 powder blend, compared to the PH1 powder, is its higher bulk density. The bulk density of the SD251 powder is about 58% higher than for PH1 powder. The higher bulk density of the SD251 powder mixture particles allows a more compact filling of the created layer. So the distance between the powder particles is smaller for the SD251 blend than for the PH1 blend. As a result, the void space between the powder particles is smaller and this makes it possible to increase the energy which the laser transfers into the powder layer during SLM. In addition, the temperature field is better distributed, and therefore the melting temperature can be reached in a shorter time.

To maintain and increase the flowability of the powder, the SD251 powder blend was dried prior to processing in the SLM device. This step means that the residual moisture in the powder processing was less than 5 wt. %. Residual moisture increases the strength of the adhesive bonds between the powder particles and it causes a reduction in the flowability of the powder. Therefore it was necessary to keep the residual moisture value of the powder as low as possible.

2.2. Methods of experiments

The SD251 powder blend was processed using an SLM additive device. Powder blend processing parameters were based on experiments previously performed with another type of WC-Co powder blend and a literature search. *(Uhlmann, Bergmann and Gridin, 2015; Wang et al., 2002; Bricín, Špirit and Kříž, 2018; GU et al., 2006; Kumar, 2009; Pacurar and Pacurar, 2016)* Based on this research, a standard thickness of the applied material layer of 40 microns was chosen. The other parameters used are summarized in Table 2 below.

Experimental material	Power of laser (W)	Scanning speed (mm/s)	Scanning distance (mm)	Thickness of layer (mm)	Atmosphere	Residual moisture (Wt. %)
SD251	250	250-1000	0.12	0.04	Nitrogen	<5

Table 2. Processing parameters of SD251 powder blend

Metallographic analysis, chemical composition analysis and X-ray analysis of the phase composition of the printed samples were then performed. The aim of these analyses was to determine how the selected parameters for processing the powder blend affect the final properties of the prototype samples. Metallographic analysis was performed using a CarlZeiss Observer Z1m light microscope and Philips XL-30 ESEM and TESCAN MIRA3 scanning electron microscopes. Metallographic analysis was used to determine the volume, size and shape of the pores in the sample structure. In addition to analysing the porosity of the samples, the aim of the metallographic analysis was to determine any changes in chemical composition and structural and phase composition of the prototype samples.

Metallographic analysis was supplemented by X-ray diffraction analysis of the phase composition and analysis of the mechanical properties of the prototype samples. The Vickers hardness test was used to evaluate the changes in the mechanical properties of the prototype samples.

3. RESULTS AND DISCUSSION

During the processing of the powder mixture, a large number of droplets were formed which flew off from the moving laser beam. This material was removed from the chamber for further analysis, see Figure 5. Analysis revealed that it was partly composed of particles of the original powder, particles in which interaction with the laser had occurred, and entirely new particles that arose due to the instability of the molten region of the powder bed.

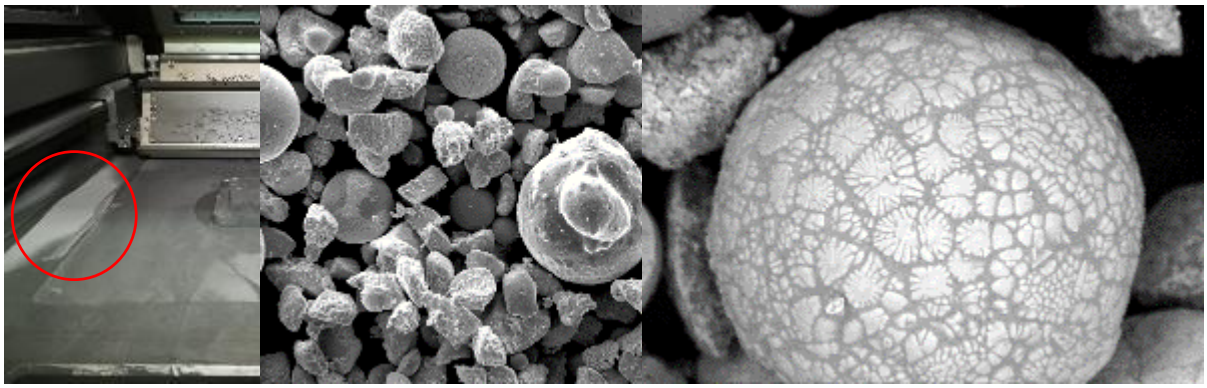

Fig. 5. The left part of the figure shows the area from which the sample for metallographic analysis was taken. The middle part of the figure shows the types of powder particles found in the sample. The sample contained particles of the original powder, particles that had been partially in contact with the laser beam, and particles that originated from the melt, see the image on the right.

The formation and number of these flying particles from the powder bed melting point is due to the phenomenon called the ‘balling effect’. *(Zhou et al., 2015)* As has been described for other types of materials, the intensity of this phenomenon is dependent on the properties of the material being processed, i.e., its chemical composition, geometric characteristics, and physical properties. The second factor that initiates this phenomenon are poorly adjusted powder mixture processing parameters.

The large number of powder particles that originated from the molten powder bed was probably associated in particular with poorly adjusted process parameters. This phenomenon occurs when the laser power used is large enough to create a large melt volume, but the speed of the laser is too high. In this case, due to the applied surface tension on the interface of the liquid, solid and gaseous phases, some of the melt forms into droplets, which then fly away from the molten area due to the excessive amount of applied input energy. The intensity of the phenomenon is greater with a faster movement of the laser beam.

Thus, the balling effect contributes to the formation of porosity in the prototype specimen body. In order to reduce the effect of this phenomenon on the samples, it was necessary to reduce the feed rate of the laser spot. As a result, it was possible to create prototype samples of sufficient quality for further analyses, see Fig. 6.

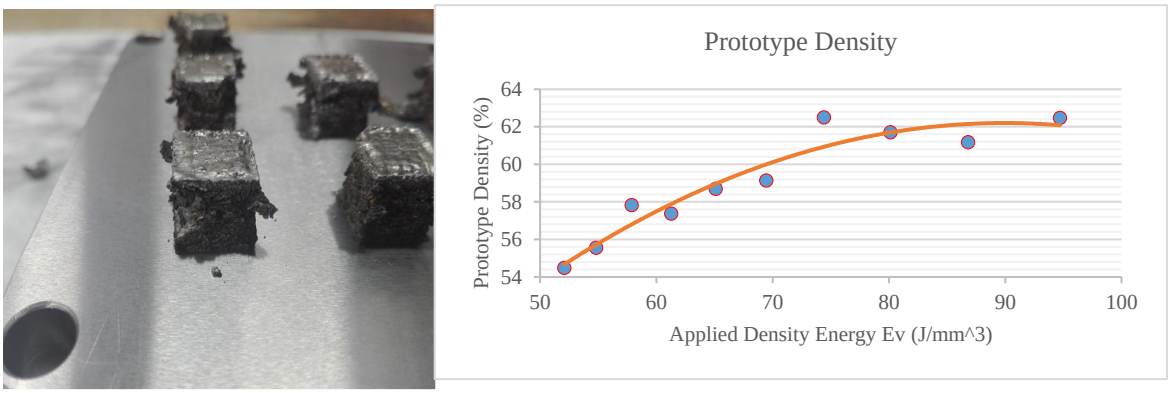

Fig. 6. On the left is a photograph of the samples after removal from the SLM chamber. The graph shows the change in sample density due to the change in applied energy Ev.

From the graph in Fig. 6, it can be seen that the density of the prototype samples increased when the laser spot speed was reduced. The maximum sample density was about 62 percent. Higher sample density values were not reached. This was because a further decrease in the speed of the laser spot caused tearing of the edges of the samples, see Figure 6. The tearing is probably associated with high residual stresses due to the rapid cooling of the molten bed. The tearing of the edges of the samples adds to the high porosity of the samples, see Fig. 7.

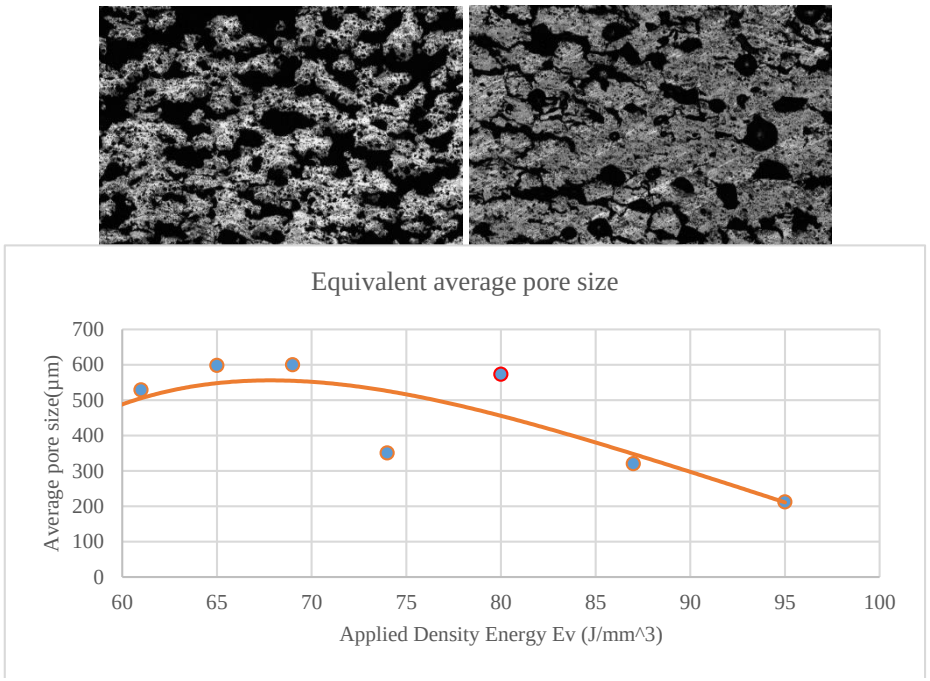

Fig. 7. Influence of applied energy on development of porosity of prototype samples. The upper left part of the figure shows the porosity of the sample at a scanning speed of v = 950 mm / s. The right part of the image shows the porosity of the sample at the scanning speed of v = 280 mm / s. Other parameters were kept constant. The graph shows how the applied energy affects the pore size

It can be seen from Figure 7 that the pores have been gradually closed by 'necks' growing between the particles of the powder due to the increasing amount of input energy. This resulted in a gradual reduction of the pore size, which is represented in the graph by a change in the pore equivalent diameter.

The porosity of samples made from the SD251 powder blend was also affected by the amount of evaporated binder and changes in the phase and structural composition of the prototype samples, see figures 8 and 9 and Table 3. Changes in binder volume were measured by EDX analysis. The difference in the volume of the vaporised binder depended on the degree of energy applied. At high applied energy values Ev = 450-550 (J / mm^3), the volume of vaporised binder ranged between 20-26 wt. %. At low values of applied energy, for example by reducing the laser power or increasing the speed of the spot movement, the volume of the evaporated binder decreased to about 13 wt. %. Fig. 8 shows a comparison between the phase composition of the SD251 powder and the phase composition of a sample made from SD251 powder measured by X-ray diffraction analysis.

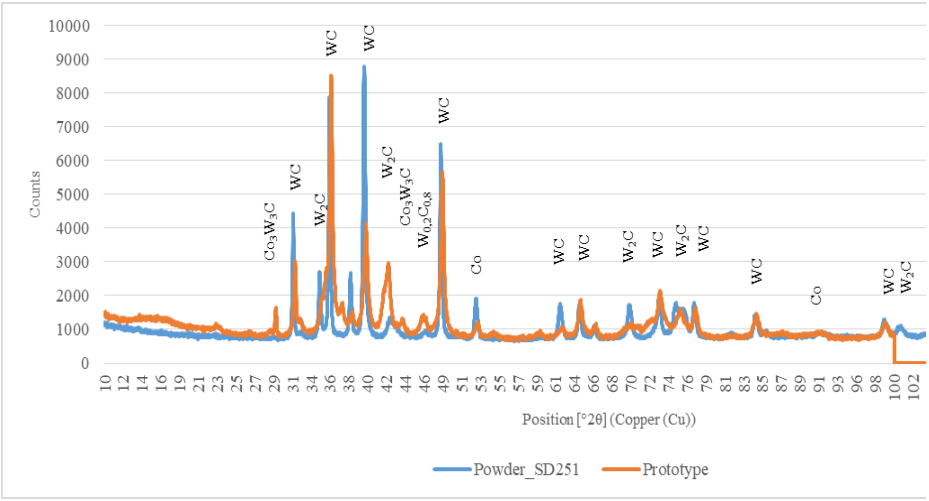

Fig. 8. Comparison of the phase composition of a sample obtained from processing SD251 powder mixture by SLM technology and the phase composition of the SD251 powder.

From Fig. 8, it can be seen that due to the diffusion of substitution and interstitial elements (carbon and tungsten) during melting of the powder bed, the proportion of tungsten carbide WC and W_2C decreased in the volume of the analysed sample. In addition, the volume growth of the Co_3W_3C phase and the $W_{0.2}C_{0.8}$ intermetallic phase occurred. It can be seen from the metallographic section (see Fig. 9), that after processing the SD251 powder mixture, the volume of Co is not found in its original form but in the form of a solid solution of $W_{0.2}Co_{0.8}$ and the structural phase of Co_3W_3C.

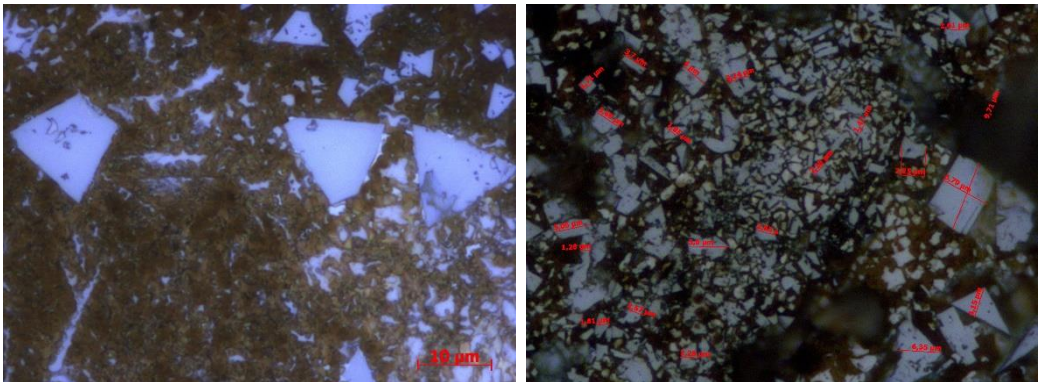

Fig. 9. Metallographic image of sample structure. The surface of the metallographic sample was etched to identify the eta phase of Co3W3C. Light grey to blue formations indicate areas of tungsten carbide grains. The orange-brown areas indicate the eta phase.

It is also evident from the metallographic images that the structure of the samples is highly heterogeneous. In the evaluated regions it was possible to see areas containing only the structural phase of Co3W3C. On the other hand, in the sample structure there were also areas where carbide grains created clusters with a huge variety of sizes. The average carbide grain size increased by about 150% in the prototype samples. The heterogeneity of the sample structure and the high porosity affected the hardness measurement. Hardness measurements indicate that the samples have low hardness and low strength bonds between the sintered parts due to their high porosity and a high proportion of the brittle phase of Co_3W_3C compared to sintered carbide made in the conventional way.

4. CONCLUSIONS

A maximum density of about 62% was achieved with the prototype specimens produced at an applied energy of 95 J / mm 3. Higher densities were not achieved because with higher applied energy values there was significant tearing of the specimens, especially at the corners, which caused the samples to disintegrate throughout their volume, making it impossible to analyse them further.

The first reason for the origination of these cracks was probably the initiation of high residual thermal stresses in the volume of the samples due to the rapid solidification of the molten powder bed. The second reason for their formation was probably the volume changes of the samples, which were caused by the formation of new structural phases and their volumetric growth. The high porosity of the samples was also due to the samples being made with a too high velocity of the laser beam which led to the creation of droplets of molten powder flying from the powder bed. This phenomenon is the 'balling effect'. Metallographic analysis of the samples confirmed that the cobalt structural phase had been converted into the eta phase of Co3W3C. Furthermore, X-ray diffraction analysis showed the presence of the phase W0.2C0.8. In addition to the structural changes in the samples made of SD251, coarsening of tungsten carbide grains, up to 150% of the original grain size, was observed. Depending on the energy applied, the volume of the binder was reduced by vaporizing. This amount of evaporated binder ranged from about 13 wt. % to 26 wt. %. In addition to poorly selected processing parameters for the powder blend, the high porosity of the prototype specimens was due to inappropriate geometry of the powder particles, which deteriorated its dosing capability on the building plate of the additive device. Another factor which affected the workability of the powder blend was the unsuitable phase composition which, unlike the powder mixture analysed in previous experiments, contained a high amount of eta phase.

Considering all the phenomena described above, it is basically impossible to make a functional part from powder mix SD251. Therefore, the next phase of the experimental programme will be focused on the suitability of other types of WC-Co powder mixtures for SLM. In order to limit the balling effect, further experiments will be performed at slower scanning rates and lower applied power laser values. As a result, with a suitable WC-Co powder blend, a functional machine component such as a cutting tool with an integrated channel assembly could be created to increase its service life by significantly reducing heat dissipation from the face and back of the tool.

ACKNOWLEDGMENTS

This experimental study was supported by the TAČR technology agency, project Zéta TJ020000218 'Production of machine tool with additive SLM technology'. This study was developed in cooperation with the Technical University of Liberec, the Institute for Nanomaterials and New Technologies.

REFERENCES

1. Venuvinod, P. and Ma, W. (2010). Rapid prototyping. Boston: Kluwer Academic
2. Uhlmann, E., Bergmann, A. and Gridin, W. (2015). Investigation on Additive Manufacturing of Tungsten Carbide-cobalt by Selective Laser Melting. Procedia CIRP, 35, pp.8-15.
3. Wang, X., Laoui, T., Bonse, J., Kruth, J., Lauwers, B. and Froyen, L. (2002). Direct Selective Laser Sintering of Hard Metal Powders: Experimental Study and Simulation. The International Journal of Advanced Manufacturing Technology, 19(5), pp.351-357.
4. Bricín, D., Špirit, Z. and Kříž, A. (2018). Metallographic Analysis of the Suitability of a WC-Co Powder Blend for Selective Laser Melting Technology. Materials Science Forum, 919, pp.3-9.
5. Bricín, D. and Kříž, A. (2018). Assesment of usability of WC-Co powder mixtures for SLM. Manufacturing Technology.18(5), pp. 727-731

6. Gu, D., Shen, Y., Dai, P. and Yang, M. (2006). Microstructure and property of sub-micro WC-10 %Co particulate reinforced Cu matrix composites prepared by selective laser sintering. Transactions of Nonferrous Metals Society of China, 16(2), pp.357-362.
7. Kumar, S. (2009). Manufacturing of WC–Co moulds using SLS machine. Journal of Materials Processing Technology, 209(8), pp.3840-3848.
8. Zhou, X. Liu, X., Zhang, D., Shen, Z. and Liu, W. (2015). Balling phenomena in selective laser melted tungsten. Journal of Materials Processing Technology, 222, pp. 32-44
9. Pacurar, R. and Pacurar, A. (2016). Applications of the Selective Laser Melting Technology in the Industrial and Medical Fields. New Trends in 3D Printing.
10. Sutton, A., Kriewall, C., Leu, M. and Newkirk, J. (2016). Powder characterisation techniques and effects of powder characteristics on part properties in powder-bed fusion processes. Virtual and Physical Prototyping, 12(1), pp.3-29.
11. Sarin, V. (2014). Comprehensive Hard Materials. Elsevier.
12. Kríž, A. and Bricín, D. (2017). Properties and Testing of Cemented Carbides. Powder Metallurgy - Fundamentals and Case Studies.
13. 18, A. (2019). ASTM B657 - 18 Standard Guide for Metallographic Identification of Microstructure in Cemented Carbides. [online] Astm.org. Available at: https://www.astm.org/Standards/B657.htm [Accessed 2 Apr. 2019].